Evaluation of Time Domain Propagation Measurements of UWB Systems Using Spread Spectrum Channel Sounding

Amir Dezfooliyan, *Student Member, IEEE*, and Andrew M. Weiner, *Fellow, IEEE*

***Abstract*—Spread spectrum sounding experiments for indoor wireless channel over a frequency band spanning 2–12 GHz, which exceeds the full FCC UWB band, are reported. Experiments were carried out for directional spiral antennas in line-of-sight (LOS) and omnidirectional biconical antennas in nonline-of-sight (NLOS) environments, in the latter case with up to 15 m antenna separation. For biconical antennas, channel multipath dispersion is the main reason for the delay spreads, while for spirals, frequency-dependent delays of the antennas modify signals upon radiation and reception. A special emphasis of this work is to assess the accuracy of the measured impulse responses extracted from the received waveforms by deconvolution in a typical indoor environment. In one scheme to assess accuracy, impulse responses obtained using different spread spectrum waveforms are compared; independent measurements show excellent agreement, with correlation coefficients about 0.99. In a second assessment approach, accuracy is tested by performing time reversal experiments based on the measured channel impulse response. Correlation coefficients between experimental and theoretical time-reversal traces are on the order of 0.98, which further confirms highly accurate measurements.**

***Index Terms*—Directional antenna, channel propagation measurement, omnidirectional antenna, spread spectrum, time-domain techniques, time reversal, ultrawidebandwidth (UWB).**

I. Introduction

ULTRAWIDEBAND (UWB) communication [1]–[3] has been studied extensively in recent years due to its potential capabilities in short range, high speed wireless applications such as covert communications, high multiple access capabilities, and wireless USB. Characterizing the wideband propagation channel is important for radio system design and performance analysis in general, and characterization of ultrawideband channels in particular, is a topic of current interest [1]. UWB comes with several unique advantages (i.e., multipath fading robustness [4], and ultrahigh range resolution for radar applications [5]), and understanding the propagation channel is prerequisite to evaluating any UWB system. Channel impacts on multiantennas system, body area networks, and ranging are discussed in [6].

Manuscript received February 02, 2012; revised April 18, 2012; accepted May 01, 2012. Date of publication July 10, 2012; date of current version October 02, 2012. This work was supported by the Naval Postgraduate School under Grant N00244-09-1-0068, and under the National Security Science and Engineering Faculty Fellowship Program.

The authors are with the School of Electrical and Computer Engineering, Purdue University, West Lafayette, IN 47907 USA (e-mail: amir@purdue.edu; amw@ecn.purdue.edu).

Color versions of one or more of the figures in this paper are available online at http://ieeexplore.ieee.org.

Digital Object Identifier 10.1109/TAP.2012.2207358

In general, there are two possible methods for wideband channel sounding and propagation measurements: frequency domain and time domain. Frequency domain measurements rely on the utilization of a vector network analyzer (VNA) which controls a synthesized frequency sweeper. The sweeper excites the channel by sinusoidal waveforms at different frequencies and records the frequency dependent S-parameter $S_{12}(f)$, which provides an estimate of the channel transfer function $H(f)$. The impulse response $h(t)$ can be calculated by taking Inverse Fourier Transform of $H(f)$. While the frequency domain approach can be used to characterize channel responses over a large bandwidth, the sweep time of the VNA ranges typically from several seconds to several minutes, depending on many factors like measurement bandwidth, speed of the synthesizer, and bandwidth of the IF filter [7], [8]. Although this suffices for time invariant channels in which the transmitter and the receiver are static, the sweep time of a VNA is too slow to handle fast time variant channels [1]. Another drawback is that complete channel characterization requires measurements of phase as well as magnitude, which in turn necessitates simultaneous connection of the VNA to both the transmitter (Tx) and the receiver (Rx). Usually this requires a high-quality doubly shielded RF cable which is a major limitation for long distance measurements. In one recent example, Pagani and Pajusco [9] used a VNA to cover the full 3.1–10.6 GHz UWB band in LOS as well as NLOS environments up to 20 m of Tx-Rx separation. Most other examples report measurements at less than 10 m of antenna separation or cover less than the full FCC UWB band [10]–[12].

Time domain measurements provide a more direct characterization approach. In the simplest case, channels are excited by a short pulse and impulse responses are sampled at the receiver end by an oscilloscope. The chief limitation of this technique is that generating ultrashort, low ringing pulses with sufficient power to measure high attenuation channels is difficult. Received responses in this method are the convolution of a channel response and a probing pulse. Deconvolution can be applied to generalize the result; however, care is required to avoid numerical instabilities [13], [14]. UWB channel measurements by using short pulses have been presented in [15]–[17]. In [16], wireless personal area network (WPAN) was studied over the frequency band of 3.1–10.6 GHz by probing the channel with narrow pulses $\sim$50 ps in duration. Measurements were conducted at short distances only up to 135 cm for both LOS and NLOS scenarios. In [17], indoor UWB channels were characterized for both LOS and NLOS cases by using a Gaussian-like waveform with approximately seven volt amplitude peak. Al-

though the pulse width is reported as less than 100 ps, no information is provided about the achieved measurement bandwidth as affected by increasing Tx-Rx propagation distances. In general, path loss is expected to be frequency dependent; and measurement of the channel response at high frequencies degrades as the distance between antennas increases.

Another time domain approach for measuring the impulse response of the propagation channel exploits spread spectrum sounders. This method has its roots in chirped radar technology, in which spread spectrum transmit signals, coupled with pulse compression at the receiver, circumvent the tradeoff between transmit energy and range [18], [19]. In this method, channels are probed by a wideband signal such as PN or multicarrier spread spectrum waveforms [20]–[22]. These signals have low peak-to-average ratio, and higher levels of total transmitted power compared to ultrashort pulses, which results in higher dynamic range. The autocorrelation of these wideband signals can ideally approach a Dirac Delta function with very low sidelobes [23]–[25]. In a number of papers in the UWB literature, the channel response has been obtained by calculating the cross-correlation of the waveform measured at the receiver with the transmitted waveform. For example, Durantini *et al.* [26], [27] used a carrier at 4.78 GHz modulated by a PN-sequence to perform channel measurements over a 3.6–6 GHz frequency band for distances ranging between 4–7.5 m for NLOS channels and 1–11 m for LOS channels. In [28], [29], a transceiver setup based on SiGe-circuits is reported to generate periodic m-sequence waveforms covering a baseband frequency range of approximately 0–5 GHz, which can be up converted to cover either the UWB band or for coverage in the 60 GHz band. Receiver consists of a down-convertor, a track-and-hold circuit, and an analog to digital convertor (ADC) which uses periodic subsampling at a rate below Nyquist. To achieve accurate subsampling and also up/down-conversion, careful synchronization is required. This transceiver is commercially available as a robust box in [30].

In this paper, we perform spread spectrum channel sounding using signals from an arbitrary waveform generator (AWG). The AWG not only provides sufficient bandwidth for channel characterization over a frequency band spanning 2–12 GHz, which exceeds the full FCC UWB band, but also provides the flexibility to choose different spread spectrum waveforms for sounding. This allows us to assess the accuracy of our channel measurements to an extent which, to the best of our knowledge, has not previously been reported in the UWB literature.

Experiments were carried out indoors, both for directional antennas in line-of-sight (LOS) environments and omnidirectional antennas in nonline-of-sight (NLOS) environments, in the latter case with up to 15 m antenna separation. Because of the practical difficulty of producing sounding signals with an ideal delta function autocorrelation, equivalent to a white power spectrum, it is important to account for the source spectrum in extracting the system impulse response. Because our experiments achieve good SNR over the full measurement band, we are able to employ a simple deconvolution procedure to accurately extract the impulse response. A special emphasis of our work is to assess the accuracy of our time domain measurements in typical indoor environments. Both spiral and biconical antennas (arranged in either copolarized or cross-polarized orientation) are considered. In one scheme to assess the accuracy of our measurements, we compare channel responses obtained using two different common spread spectrum waveforms, PN sequences and chirp signals. We show despite their well known different characteristics [31], under our channel environments, independent measurements show excellent agreement, with correlation coefficients about 0.99. In a second assessment approach, accuracy is tested by performing time reversal (TR) [32]–[35] experiments based on the measured channel impulse response. Here the time reversal experimental results are compared with the simulation trace that shows what should ideally be measured at the receiver in the time reversal experiment if there is no noise and if our impulse response measurements are perfectly accurate. Here the correlation coefficients between experimental and theoretical time-reversal traces are on the order of 0.98, which further confirms measurement accuracy. To the best of our knowledge, this is the first experimental report of TR over the whole UWB FCC mask. Other experimental TR literatures either cover a small portion of the UWB [35], or are completely out of the main UWB band (3.1–10.6 GHz) [34].

We note that in general, path loss is frequency dependent and high frequencies experience more attenuation than low frequencies, especially in NLOS environments [36]. Therefore, exciting the channel by a waveform covering a specified frequency band does not guarantee signal-to-noise sufficient to measure the channel response over the entire band. In this paper, we make a point to report power spectra not only of transmitted channel sounding signals, but also of the resulting signals measured at the receiver. In contrast to many time domain channel response measurements reported in the literature, this practice helps to more fully specify the band over which impulse responses are characterized.

In many of our experiments, we introduce a simple optical fiber link to achieve synchronization between transmitter and receiver. This facilitates achieving high quality synchronization, even in NLOS cases with transmitter and receiver placed in different rooms with up to 15 meters of separation.

The remainder of this paper is organized as follows: Section II provides details of the physical measurement setup. Section III describes our measurement methodology, including the characteristics of the transmitted sounding signals and the processing algorithm employed to extract the impulse responses. Examples of measurement results are reported in Section IV, both for spiral and omnidirectional antennas. Finally, in Section V we conclude.

II. Experimental Setup

Fig. 1 shows a block diagram of the measurement system. The main components of the transmitter block are an AWG, ultrabroadband amplifier, and the transmitting antenna. We used our Tektronix AWG 7122B in interleaving, zeroing-on mode, which provides the maximum available bandwidth. In interleaving mode, signals from two 12 GS/s D/A channels are offset in time by half of the sampling period and passively combined to reach a maximum sampling rate of 24 GS/s. Interleaving also permits two modes of operation, zeroing on and zeroing off, which determine how individual samples are

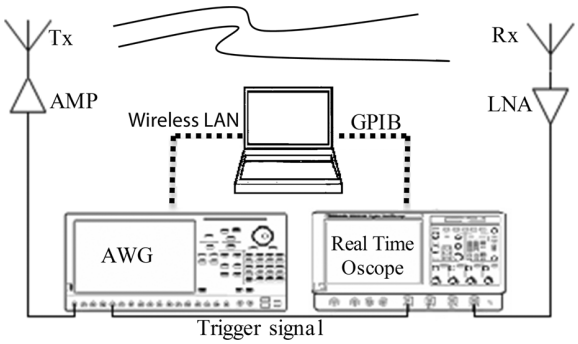

Fig. 1. Block diagram of the measurement system.

handled. In zeroing-off mode, the two D/A channels provide nonreturn-to-zero waveforms which are summed together. With zeroing on, each waveform is brought to zero before the next sample, and the output signal is the summation of the two waveforms with zero gaps between samples. Zeroing on has higher frequency response in comparison with zeroing off, but the maximum output amplitude is reduced from 1 V_{P-P} to 0.5 V_{P-P}. The AWG in interleaving, zeroing-on mode has an effective RF bandwidth (-6 dB) of 9.6 GHz, with a rise and fall time (20% to 80%) of 35 ps. The output of the AWG is amplified by an ultrabroadband amplifier (Picosecond Pulse Labs 5828A) with 10 dB gain, 6 dB noise figure, 12 dBm maximum output power and 14 GHz bandwidth. We have used two different antennas in our experiments: Directional Archimedean spiral antennas (NURAD 9C41600, 2–18 GHz), which are strongly dispersive and have circular polarization, and wideband omni-directional antennas (ELECTRO-METRICS EM-6865, 2–18 GHz) which have vertical polarization and uniform radiation pattern in the azimuth plane. The EM-6865 is composed of two brass biconical elements which are connected point-to-point and make up an antenna element shaped like a vertical infinity symbol.

The received response of the Rx antenna is passed through a Low Noise Amplifier (LNA) (B&Z Technologies, BZP120UD1). The selected LNA has a flat frequency response over 0.1–20 GHz, a 2.2 dB noise figure and a minimum 31 dB gain. Depending on the Tx-Rx distance, antenna type (directional or omni-directional) and environment (LOS/NLOS), channel loss varies significantly, and for some experiments we choose to add up to two more amplifiers on the receiver side. These amplifiers are identical to the ultrabroadband amplifier used on the transmitter side. Such additional amplification is particularly important for receiving high RF frequencies which experience more attenuation. In cascading amplifiers, it is important to avoid amplifier saturation, which in our experiments arises due to interference from Wi-Fi wireless signals with frequency of 2.44 GHz. Hence, when extra amplifiers are used at the Rx, a high pass filter is used after the LNA. This filter (Mini-Circuits, VHF-3100+) has approximately constant transmission over the 3–11.5 GHz band and roughly 43 dB insertion loss at 2.44 GHz, which is sufficient to avoid saturation due to Wi-Fi signals.

The received signal after amplification is directly connected to the real-time oscilloscope (Digital Serial Analyzer, Tektronix DSA 72004B) with 20 GHz analog bandwidth and maximum real-time sampling rate of 50 GS/s. The "average" data acquisition mode, in which we average over 256 measurements, is used to reduce additive noise. The data acquisition time is approximately 400 ms, dominated by oscilloscope dead-time between successive measurements in averaging mode. The oscilloscope is triggered by one of the AWG's digital "marker" outputs which is synchronized with the transmitted waveform with timing jitter below 30 ps and a rise/fall time (20% to 80%) specified to be 45 ps. For short Tx-Rx distances ($\leq$6 m), the trigger signal is sent to the oscilloscope by a coaxial cable. As the distance between antennas increases, particularly for NLOS environment where we have to pass the cable through the doors, the loss and dispersion in the cable results in higher jitter [17]. To solve this problem, we use a single-mode optical fiber link (0.2 dB/km optical loss [37]) to transfer the trigger signal. A continuous-wave (CW) optical signal at 1.55 μm wavelength from a tunable laser (Agilent 81689A) is directed into a commercial lithium niobate intensity modulator (IM) with DC electrical bias adjusted for roughly 50% transmission and with an amplified version of the AWG marker signal connected to the RF input of the IM. This creates an optical intensity modulation that mirrors the electrical marker signal [37]. The modulated optical signal is connected through fiber to a high speed photodetector (THORLABS DET01CFC, 2 GHz RF bandwidth) which provides the high speed electrical signal for triggering the oscilloscope.

Signals recorded by the oscilloscope are stored on a personal computer using a GPIB interface. For NLOS experiments the operator is typically positioned in the same room as the Rx. The AWG is controlled remotely over a wireless local area network.

Measurements have been carried out in the subbasement of the MSEE building at Purdue University. Channel propagation is studied in different locations for omni-directional and spiral antennas to prove the accuracy of our measurements in several independent experiments. For omnidirectional case, we measured LOS and NLOS scenarios. LOS experiments were conducted in a large laboratory (15 m $\times$ 10 m) which contains metallic desks, cabinets, computers and scattering objects of different sizes. For NLOS measurements, we placed the transmitter in the laboratory and the receiver in an office across from the laboratory, and there are two cement walls and a hallway in the direct path of the Rx-Tx antennas. As we mentioned, the omnidirectional antenna has vertical polarization and uniform radiation in the azimuth plane. We conducted our measurements in two different copolar and cross-polar topologies for omnidirectional antennas. In copolar experiments, both the Tx and Rx have the same vertical polarization, while in cross-polar measurements, the Tx and Rx have different polarization directions (we rotated the Rx antenna 90° degrees to have horizontal polarization). For spiral antennas, different situations were studied, including LOS, NLOS in the same room by pointing antennas to different directions, and NLOS by placing antennas in different rooms. In this paper, we present our channel measurement method in detail for the LOS spiral and NLOS copolar omni-directional cases. We have chosen these two examples because different physical interactions are mainly involved in these two experiments. In the NLOS omnidirectional case, the transmitted signals from the Tx can be propagated in all direc-

TABLE I
CORRELATION COEFFICIENTS FOR IMPULSE RESPONSES MEASURED BY PN AND CHIRP EXCITATIONS, AND ALSO FOR SIMULATION AND EXPERIMENTAL TR FROM CHIRP EXPERIMENTS. *: FOR OMNIDIRECTIONAL ANTENNAS, WE USE "LOS" TO MEAN THAT ANTENNAS ARE IN THE SAME ROOM, WITH NO OBSTRUCTION BETWEEN THEM. HOWEVER, NOTE THAT CROSS-POLAR RESPONSE ARISES FROM SCATTERING

Environment Type	Correlation coefficient between impulse responses measured by PN and chirp excitations	Correlation coefficient between simulation and experimental TR
Spiral LOS	0.997	0.974
Spiral NLOS	0.995	0.976
Omni-directional co-polar LOS	0.997	0.986
Omni-directional cross-polar LOS *	0.995	0.987
Omni-directional co-polar NLOS	0.991	0.978
Omni-directional cross-polar NLOS	0.990	0.975

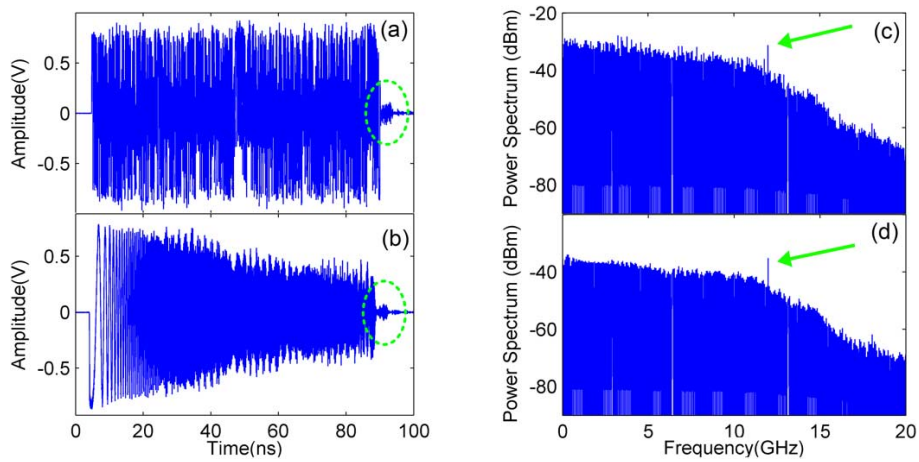

Fig. 2. (a), (b) Generated PN and chirp signals in time domain, respectively. Both the PN and chirp waveforms have a nominal duration of 85.3 ns. (c), (d) RF power spectra of the generated PN and chirp signals, respectively. Resolution bandwidth of spectrum analyzer is 100 KHz. Both signals are defined over the frequency range of 0–12 GHz. Indicated parts by ellipsoids show extra features produced by AWG due to RF reflections in interleaving zeroing mode. The RF spectra also exhibit a spur at 12 GHz, equal to the individual channel sample rate of the AWG. These spurs are shown by arrows.

tions and reach the Rx via different paths and interactions (e.g., reflection, diffraction or scattering). The received response in this experiment mainly consists of different components which have certain delays and attenuations due to the paths they took in their propagations from the Tx to the Rx. In the LOS spiral experiment, antenna distortions, especially dispersion, affect the received response, and the measured impulse response is mainly antennas' dispersion. In addition to the results of these two specific scenarios which are presented in detail, the accuracy of measurement performed in several other scenarios is tabulated in Table I, which is discussed later.

III. MEASUREMENT METHOD

A. Probe Signals

We used PN sequences and chirp signals for channel sounding and studying accuracy of our measurements. PN sequence can be easily generated by a switching circuit (e.g., SiGe circuits [29]) and is the most common waveform used in spread spectrum channel sounding. In the experiments here, we used the AWG to generate a maximal length PN sequence with 2047 chips and a 24 GHz chip rate, corresponding to a waveform duration of $\sim$85.3 ns. The chirp signal used in our experiments is a linear swept-frequency sinusoid whose frequency increases in time (up-chirp) from 0 to 12 GHz over the same 85.3 ns time aperture used for the PN-sequence. In both cases the AWG is programmed to generate the selected waveforms periodically at 2.4 MHz repetition rate to support averaging. Received waveforms are recorded with 20 ps sampling resolution over a sufficiently long time window (400 ns) to include all multipath components. This corresponds to 20 000 data points per waveform, which can be easily stored in our real-time oscilloscope with memory length of 250 Megasamples.

Fig. 2(a) and (b) show generated PN and chirp waveforms after amplification by the Tx ("ultrabroadband") amplifier and direct connection to the oscilloscope through a DC-18 GHz triple shielded coaxial cable. Fig. 2(b) shows the chirp waveform rolls off in time and its amplitude decreases. This can be explained by considering time-frequency characteristics of our chirp signals, for which the frequency increases linearly with time. Due to the frequency response of the AWG, the later, high frequency components of the signal are generated with lower amplitude than the earlier, low frequency components. Hence, the roll-off in time simply reflects the frequency response of the AWG generating the chirped signal. In contrast, for the PN signal high and low frequencies are present concurrently, and such gradual roll-off in time is not observed. Fig. 2(c) and (d) display the RF spectra of the amplified transmit waveforms, measured by an RF spectrum analyzer set for 100 KHz resolution bandwidth. Here the high frequency rolloff of the AWG is apparent for both waveforms. The RF spectra also exhibit a spur at 12 GHz, equal to the individual channel sample rate of the AWG. These spurs may arise to differences in the amplitudes of the individual AWG channels or due to inaccuracy in

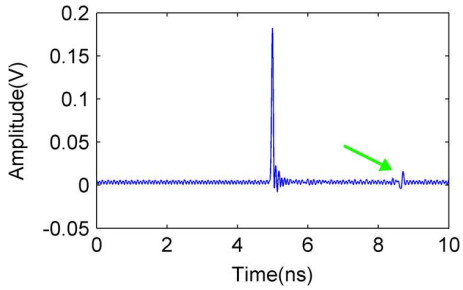

Fig. 3. Impulse signal generated by AWG with the minimum possible rise time (FWHM is $\sim$50 ps). The indicated part by the arrow shows the extra feature produced by AWG due to RF reflections in interleaving zeroing mode.

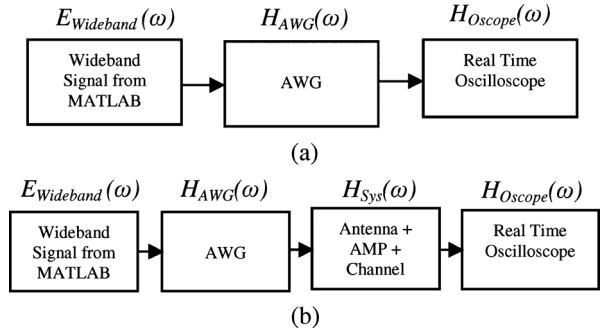

Fig. 4. Block diagram of the experimental setups. (a) AWG is programmed by the wideband signal and its output is connected to the real time oscilloscope (Y_{Trans}). (b) Channels are excited by the AWG output. Impulse responses of the antennas, amplifiers and channel are included in addition to part (a) (Y_{Rec}).

the time offset of the interleaved channels. Finally, the sections of the waveforms indicated by ellipses in Fig. 2(a) and (b) highlight an additional nonideal feature present in the AWG output, namely an echo with approximately 4 ns delay that arises in interleaving mode due to an RF reflection. This replica is more obvious when the AWG is set to generate an impulse of minimum ($\sim$50 ps) duration (see Fig. 3).

B. Data Processing and Analysis

Fig. 4 shows a block diagram of the experimental setup used for extracting the impulse response of the system from the received waveform. Fig. 4(a) portrays a calibration measurement in which the sounding waveform is recorded without wireless transmission, and Fig. 4(b) portrays the measurement in which antennas, corresponding amplifiers, and the channel itself are all now included. Equations (1)–(2) below provide a frequency domain description of the calibration and channel measurements portrayed by Figs. 4(a) and (b), respectively

$$Y_{\mathrm{Trans}}(\omega) = E_{\mathrm{Wideband}}(\omega)H_{\mathrm{AWG}}(\omega)H_{\mathrm{Oscope}}(\omega) \tag{1}$$

$$Y_{\mathrm{Rec}}(\omega) = E_{\mathrm{Wideband}}(\omega)H_{\mathrm{AWG}}(\omega)H_{\mathrm{Sys}}(\omega)H_{\mathrm{Oscope}}(\omega). \tag{2}$$

Where H_{AWG} and H_{Oscope} are, respectively, the frequency response of AWG and oscilloscope, and H_{Sys} is the frequency response of the antennas, amplifiers, channel and the high-pass filter (if used in our system). E_{Wideband} denotes the ideal spread spectrum (PN or chirp) signal generated by MATLAB in frequency domain, Y_{Trans} is the output of AWG connected by a short RF cable to the oscilloscope, and Y_{Rec} includes channel, antennas, amplifiers and the high-pass filter (if used in our system) in addition to Y_{Trans}.

To extract $H_{\mathrm{Sys}}(\omega)$ from Y_{Rec}, different approaches can be employed [21], [22]. Here we compare two simple approaches, one of which takes into account the full spectral characteristics of the sounding waveform and one of which does not. Although both of the methods we consider are well known [22], [38], we discuss our implementation in detail so that interested readers can replicate our measurements if desired. Our specific formalism relies on deterministic Fourier transformable transmitted signals and we assume synchronization is maintained throughout the measurement for a periodic transmission and reception.

For ideal spread spectrum signals with a pulse-like autocorrelation, the unbiased impulse response estimation can be derived from the cross-correlation of the received response with the transmitted signal. This approach, which has been used in a number of spread spectrum channel sounding papers [25]–[28], [30], is expressed mathematically, in time and frequency domains respectively, as

$$h_{\mathrm{Sys}}^{\mathrm{XC}}(t) = y_{\mathrm{Rec}}(t) * y_{\mathrm{Trans}}^{*}(-t) \tag{3}$$

$$\begin{aligned} H_{\mathrm{Sys}}^{\mathrm{XC}}(\omega) &= Y_{\mathrm{Rec}}(\omega)Y_{\mathrm{Trans}}^{*}(\omega) \\ &= |E_{\mathrm{Wideband}}(\omega)H_{\mathrm{AWG}}(\omega)H_{\mathrm{Oscope}}(\omega)|^2 H_{\mathrm{Sys}}(\omega) \end{aligned} \tag{4}$$

where $*$ denotes the convolution operation; and y_{Rec}, y_{Trans} and $h_{\mathrm{Sys}}^{\mathrm{XC}}$ are the impulse responses related to Y_{Rec}, Y_{Trans} and $H_{\mathrm{Sys}}^{\mathrm{XC}}$ by Inverse Fourier Transform (IFT). In our notation, $H_{\mathrm{Sys}}^{\mathrm{XC}}(\omega)$ and $h_{\mathrm{Sys}}^{\mathrm{XC}}(t)$, respectively, refer to estimates of the frequency response and impulse response of the channel, antennas and amplifiers obtained via cross-correlation processing. In (3), although y_{Trans} and $h_{\mathrm{Sys}}^{\mathrm{XC}}$ are real since we are considering them to be baseband signals, we retain the complex conjugate so that (3) is also applicable to the case where y_{Trans} and $h_{\mathrm{Sys}}^{\mathrm{XC}}$ are considered as envelope functions with an assumed carrier.

In this approach only the spectral phase of the sounding signal (Y_{Trans}) is compensated; its frequency dependent magnitude still contributes to the final estimation of the system transfer function (e.g., neither the high-frequency roll-off of the AWG response, nor other irregularities in the power spectrum due to the echo in the AWG response, are compensated). As a result, when the transmitted spread spectrum signal is not white (autocorrelation is not a delta function) [20], [23], an unbiased estimation cannot be achieved using just (3) and (4). These power spectrum imperfections can easily occur in practical measurement system involving ultrawide bandwidths [26]–[29]. To illustrate, examples of our experimental autocorrelations are shown in Fig. 5 for PN and chirp transmit signals (y_{Trans}). For example, due to RF reflections internal to the AWG, the autocorrelations of both transmitted signals have unwanted peaks at approximately ± 4 ns of the main peak. Also, although the autocorrelations of ideal, periodically repeated PN-sequences (known as periodic autocorrelation) are known to have an ideal pulse like property [23], the autocorrelation of the single period of a PN-sequence which is

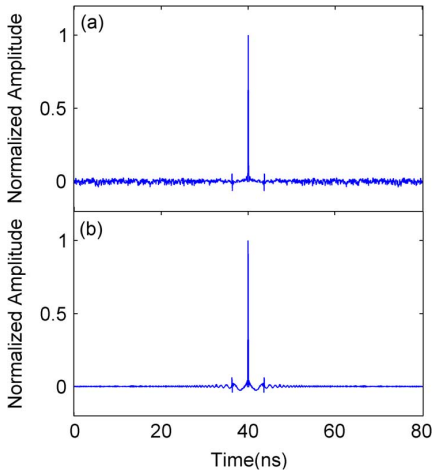

Fig. 5. Autocorrelation of (a) PN (b) chirp. Extra replicas at ∼4 ns of the main peak are due to AWG RF reflections.

used in our experiments, exhibits significant low level structure outside of the main peak [27]. On the other hand, the sidelobes of the autocorrelation of single frame chirp signals behave like a Sinc function [24] and have comparable quality to the sidelobes of periodic autocorrelation. As a result, the autocorrelations computed from our experimentally measured transmit signals are significantly cleaner for the chirp waveform than for the PN waveform, though neither is ideal. Because of such practical issues, the quality of impulse responses computed via (3) and (4) will be compromised, since the nonideal autocorrelation and power spectrum of the sounding waveform are not taken into account.

A simple approach that does take into account the full source characteristics is deconvolution [21], [22]. The deconvolution operation can be performed either in the time [13], [14] or frequency domain; here we operate in the frequency domain by the application of the fast Fourier transform. Symbolically, we can write

$$H_{\mathrm{Sys}}(\omega) = \frac{Y_{\mathrm{Rec}}(\omega)}{Y_{\mathrm{Trans}}(\omega)} \tag{5}$$

$h_{\mathrm{Sys}}(t)$ can be computed from $H_{\mathrm{Sys}}(\omega)$ by inverse transform

$$h_{\mathrm{Sys}}(t) = \frac{1}{2\pi}\int_{-\infty}^{+\infty} H_{\mathrm{Sys}}(\omega)e^{j\omega t}\,d\omega. \tag{6}$$

We use the notation $H_{\mathrm{Sys}}(\omega)$ and $h_{\mathrm{Sys}}(t)$, without superscript, to refer to estimates of the frequency response and impulse response, respectively, obtained via the deconvolution method, which we use throughout the rest of this paper unless otherwise noted. Although (5) and (6) are simple, they are computationally unstable around the zeros of Y_{Trans} and mathematically classified as an ill-posed problem. In general, these equations are extremely sensitive to the presence of noise, and the transmitted signals, Y_{Trans}, should maintain a good SNR over the desired spectral range. In our experiments, as the transmitted signals cover frequency range up to 12 GHz, we resample the recorded data at 24 GHz, and apply (5) to the resampled data. Because the transmitted signals have good frequency content up to 12 GHz (see Fig. 2(c) and (d)), we did not face instability problems in our computations. By implementing deconvolution in (5), modulations of the transmitted power spectrum due to system imperfections are taken out which ideally results in an unbiased estimation of the system impulse response.

For each antenna placement, we have also implemented the time reversal technique [32]–[35]. Our experimental procedure consists of resampling the obtained channel impulse response at 24 GHz, inverting the result in time, and programming this directly onto the AWG. This signal is then transmitted, and the new waveform measured at the receiver is recorded using the oscilloscope. We compare this result with the simulated signal which is the autocorrelation of the measured channel impulse response convolved with the impulse response of AWG and oscilloscope

$$y_{\mathrm{TR}}(t) = h_{\mathrm{Sys}}(-t) * h_{\mathrm{Sys}}(t) * h_{\mathrm{AWG}}(t) * h_{\mathrm{Oscope}}(t). \tag{7}$$

For these simulations we measured the impulse response of AWG and oscilloscope by dividing the spectral amplitude of the chirp signal recorded at the output of the AWG, $Y_{\mathrm{Trans}}(\omega)$, by the spectral amplitude of the ideal chirp waveform, $E_{\mathrm{Wideband}}(\omega)$. This yields a better signal-to-noise ratio in comparison with the direct impulse response measurement showed in Fig. 3. This simulation approach shows what should ideally be measured at the receiver in time reversal experiments if there is no noise and if our channel measurements are perfectly accurate. Comparing this form of simulation with the time reversal experiment provides an additional check on the accuracy of the estimated channel impulse responses.

Results for two different antenna types and propagation scenarios are discussed in Section IV.

IV. Impulse Response Measurements

A. Directional Spiral Antenna

We first measure impulse response for two spiral antennas in LOS situation which mainly includes antennas' dispersion effects. The dispersive pulse response of these spiral antennas was previously studied in [39], [40], where pulses of variable bandwidth and center frequency obtained from a photonic waveform generator were used for antenna excitation. In the experiments here, the height of the antennas is 1.8 m and their distance is 3 m to satisfy far-field conditions. Because path loss is small in this measurement, we placed just one LNA in the receiver side, in addition to the ultra-broad band AMP which we have used on the Tx side in all our experiments.

Fig. 6(a) and (b) are the received responses from PN and chirp excitations in time domain. As we mentioned, nominal duration of the probing PN and Chirp signals are 85.3 ns. Fig. 6(b) shows the received response of chirp excitation is shorter than the PN response and the transmitted signal length. This again can be explained by considering time-frequency characteristics of chirp signals. When this signal is transmitted through the antenna (which has frequency response from 2–18 GHz), the beginnings of the pulse (up to 2 GHz) are filtered out, and therefore the exciting signal becomes shorter than 85.3 ns. On

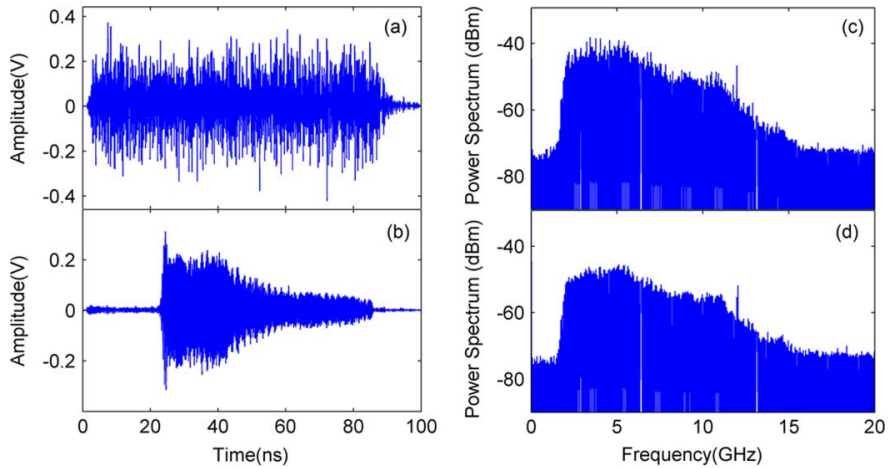

Fig. 6. Received responses from (a) PN (b) chirp. Time durations of the chirp and PN responses are ∼64 ns and ∼94 ns, respectively. (c) RF power spectrum of the received response from PN excitation (d) RF power spectrum of the received response from chirp excitation.

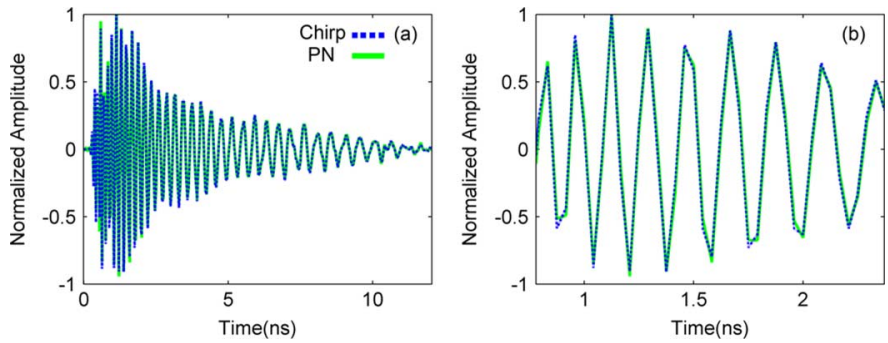

Fig. 7. Experiments using spiral antennas in a LOS topology. (a) The dotted and continuous curves are calculated impulse responses of chirp and PN excitations, respectively. (b) Zoom in on (a) to better show the agreement between two measurements.

the other hand, our spiral antennas have a strong down-chirp impulse response, while the signal generated by the AWG is an up-chirp waveform. Propagation of this up-chirp waveform through a down-chirp antenna introduces partial time domain compression [39], [40]. These two effects together result in a shorter response compared to the PN excitation experiment. In PN signals, high and low frequencies are present concurrently and transmitting this signal from antenna does not reduce the signal length in the time domain. Fig. 6(c) and (d) show RF power spectra of the received response by using Spectrum analyzer, 33 KHz bandwidth resolution. It is evident our measurement frequency range is ∼2–12 GHz. Power spectrum increases from ∼2 GHz up to ∼5 GHz then decreases fast from ∼5 GHz to ∼8 GHz and after this point is approximately constant up to 12 GHz. Comparing Fig. 6(c) and (d) with Fig. 2(c) and (d) shows spiral antennas introduce ∼8 dB more loss in frequencies around 10 GHz in comparison with the maximum frequency response around 5 GHz. These results are exactly consistent with the predicted power spectrum shape in [39] which used the same pair of spiral antennas.

Calculated impulse response from chirp and PN excitations based on (5) are compared in Fig. 7. The agreement between the two curves is excellent. By looking at Fig. 7(b) which is zoom in version of Fig. 7(a), we can see they match peak for peak and there is at most a few percent difference between them. In order to evaluate similarities between these results, it is useful to calculate the correlation coefficient. For two variables X and Y, the correlation coefficient is defined as

$$\rho = \frac{E[XY] - \bar{X}\bar{Y}}{\sigma_X \sigma_Y} \tag{8}$$

where E is the expected value, σ is the standard deviation. Ideally, in the case of $X = Y$, the correlation coefficient is equal to 1. So, when ρ is close to 1, there is a strong correlation between X and Y. In our LOS spiral antenna experiment, the correlation coefficient between two calculated impulse responses is 0.997. These results show that calculated impulse response is independent of the transmitted signals, and measurement errors are very small.

Time Reversal results for the LOS spiral antennas, in this case using the impulse response estimated based on the chirped sounding waveform, are presented in Fig. 8. Experimental measurements and simulation results are very close. Full width half maximum (FWHM) durations of simulated and experimental TR peaks are both ∼50 ps, which is equal to the FWHM of the minimum pulse that can be generated by the AWG. Fig. 8(b) shows this result over a longer time window. Both experiment and simulation show an extra feature at ∼4 ns after the main peak. This can be explained by looking at the TR simulation equation. In (7), $h_{\mathrm{Sys}}(-t) * h_{\mathrm{Sys}}(t)$ is a symmetric signal which based on our method is independent of the AWG impulse response, but when this part is convolved with

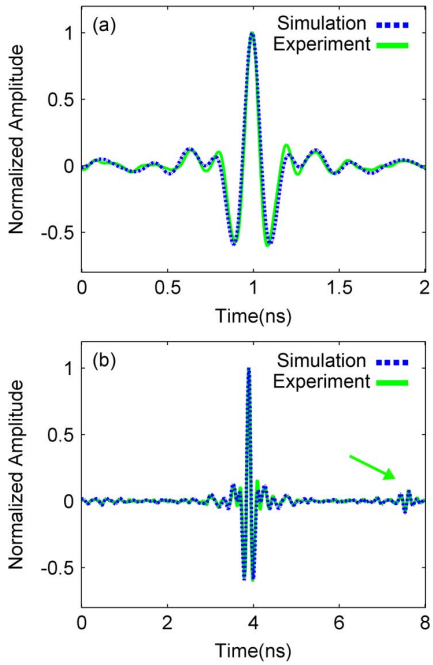

Fig. 8. Comparison between Time Reversal experiment and simulation for LOS spiral antennas over two time windows. The part indicated by the arrow corresponds to the echo in the AWG response.

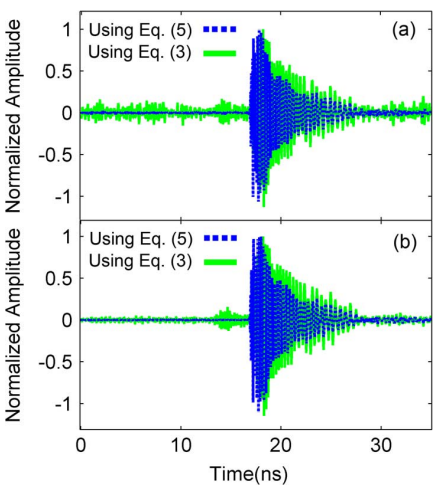

Fig. 9. Comparison between impulse responses calculated via (3) and via (5) for spiral antennas in a LOS topology. (a) PN excitation. (b) Chirp excitation.

$h_{\mathrm{AWG}}(t) * h_{\mathrm{Oscope}}(t)$, the extra replica appears after the main peak due to the RF reflection in the AWG. As we discussed in (7), the agreement between the simulation and experimental TR results shows our accuracy in measuring the impulse response of the channel, antenna and AWG. The correlation coefficient between simulated and experimental TR traces is 0.974, which shows remarkable similarity between the two data sets. We also performed TR using the impulse response measured by PN excitation, and the result is essentially indistinguishable from the TR experiment using the channel response measured by chirped excitation.

To show the importance of accounting for the actual source power spectrum in computing the actual system impulse response, Fig. 9 compares results computed on the basis of (3)–(4)

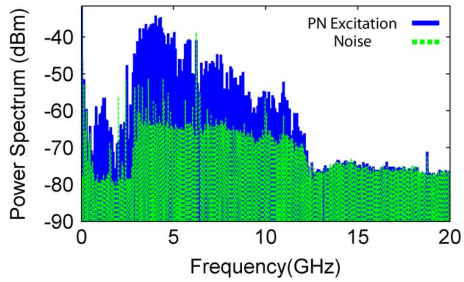

Fig. 10. Experiment using omnidirectional antennas in a NLOS environment. RF power spectrum at the receiver, after high pass filter and cascaded amplifiers. The continuous plot shows spectrum for PN excitation, and the dotted one is the noise power when the transmitter is turned off.

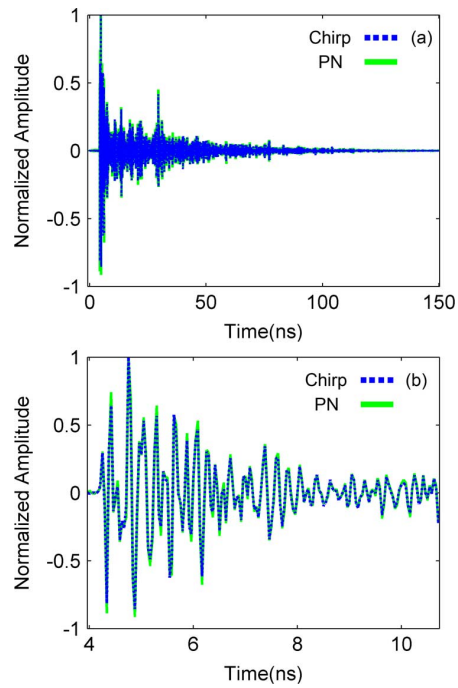

Fig. 11. Experiments using omnidirectional antennas in a NLOS environment. (a) The dotted and continuous curves are calculated impulse responses using chirp and PN excitations, respectively. (b) Zoom in on (a) to better show the agreement between two measurements.

with those computed on the basis of (5). The results are clearly different. Furthermore, the calculated responses via (3) evidently depend on the excitation signal. The impulse response using the PN waveform and (3) is noisier than that using chirped excitation. As mentioned earlier, the autocorrelation of our experimental PN sequence has noise-like sidelobes; while the autocorrelation of our chirp signals behaves like a Sinc function. Because (3) does not fully account for imperfections of practical ultrawideband sounding waveforms, estimation of impulse responses is degraded. Conversely, because (5) does account for such imperfections, extraction of the impulse response is more robust against waveform variations, provided that Y_{Trans} maintain sufficient SNR over the measurement bandwidth.

We repeated the same procedure in different locations and environments with spiral antennas to study the accuracy of our measurements in several independent experiments. For example, in a NLOS scenario, we placed the antennas in different rooms and aligned them for the maximum reception. The

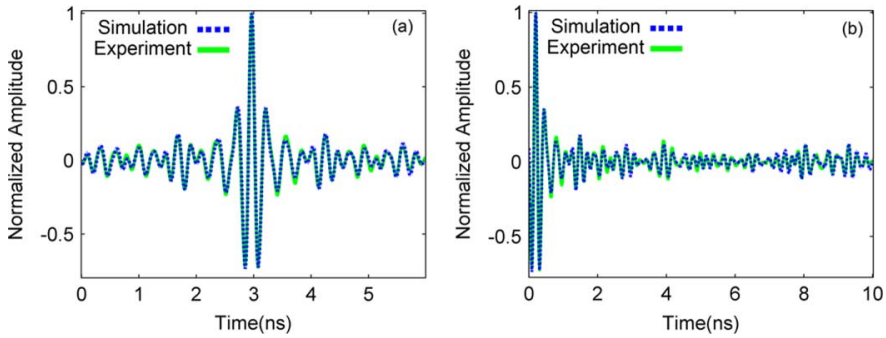

Fig. 12. Comparison between simulation and experimental time reversal technique for omnidirectional copolar NLOS environment. (a) main peak of the TR response. (b) ∼10 ns region of the TR signal following the main peak. Some parts of the peak signal can be seen on the left side of this figure.

correlation coefficient between the measured impulse responses of PN and chirp excitations in this case is 0.9953. This value for the simulation and experimental TR is 0.9766 which proves remarkable measurement accuracy even in NLOS scenarios.

B. Omni-Directional Antenna

Omni-directional antennas are the most common and appropriate antennas for wireless communication applications. NLOS channel responses for omni-directional antennas have been studied by using frequency domain channel sounding in different literatures [7], [9], [11]. Studying channel characterizations by employing pulse excitation is extremely difficult due to high channel attenuations in these scenarios. In this section, we explain NLOS copolar channel measurement over the entire UWB frequency range for omni-directional antennas by using our spread spectrum sounding technique. Antennas are located $\sim$15 m far apart, with two cement walls in their direct path, which result in high losses especially for high frequencies. To receive high frequency components and cover the full UWB frequency range, we used 51 dB gain amplification on the receiver's side. The main limitation of cascading amplifiers is the saturation effect in the final stages. Wi-Fi wireless signal is the major interference in most residential environments, with a frequency around 2.44 GHz. As explained earlier, instead of turning off the Wi-Fi transmitters, we used a high pass filter ($\sim 3 - 11.5$ GHz) which suppresses Wi-Fi signals by 43 dB. Fig. 10 shows the power spectrum of the channel excitation by the PN signal, and also the noise level when the transmitter is turned off. In these measurements, the spectrum resolution bandwidth is set to 33 KHz. It can be seen with this resolution bandwidth, the noise level is about -65 dBm which is equivalent to the noise power spectral density of -110 dBm/Hz. High UWB frequency components experience $\sim$25 dB more loss than low frequency components around 3.1 GHz. In contrast, this frequency dependence in LOS measurements ($\sim$3 m propagation distance) with the same omni-directional antennas is about 7 dB. The extra loss for high frequency components in the NLOS case is the result of passing signals through walls. In [36], experimental results show there is $\sim$10 dB loss difference between 3 GHz and 10 GHz when signals propagate through a single indoor cement wall.

Fig. 11 shows calculated impulse response for PN and chirp excitations using (5). Again, we can see the agreement between the results is remarkable and by eye is almost perfect. Again this confirms that our channel measurement is independent of the exciting signal. The correlation coefficient between these two responses is 0.991 which shows strong correlation between the two data sets.

The simulation and experiment of Time Reversal Technique, using the impulse response estimated using chirped waveform excitation, are compared in Fig. 12. Fig. 12(a) shows the main peak of the TR over a $\sim$6 ns time window. The correlation coefficient between these two data sets over 50 ns time range, which covers the main sidelobes of the TR response, is 0.978. In Fig. 12(b), we zoom in on the sidelobes of the TR response close to the main peak. Some parts of the main peak can be seen on the left side of this figure, to show the agreement between simulation and experimental results on this part of the TR. Again simulated and experimental traces curves agree quite well, which again proves that we have a very small error in estimating the physical response of our system, even in NLOS environments.

We also investigated impulse response measurements in other scenarios to study the repeatability and accuracy of the deconvolution method. Table I shows correlation coefficients for impulse responses measured by PN and chirp excitations, and also for simulation and experimental TRs based on chirp experiments. LOS and NLOS experiments were conducted in the environments described in Section II. The presented values are examples of several measurements we conducted in different locations. This technique shows comparable performance for copolar and cross-polar measurements, but, in general, LOS experiments for omni-directional antennas have higher correlation coefficient values in comparison with the NLOS measurements. This can be explained by considering the overall amplifier gain value on the Rx side in these two scenarios. In NLOS experiments, we amplified the received response by the overall 51 dB gain, however, we have lower path loss in LOS experiments and the overall receiver gain is 20 dB. Higher gain values on the NLOS receiver side results in more noise amplifications, and, therefore, the correlation coefficient between data sets is lower.

Based on our measurements, impulse response of the channels can be changed dramatically from one location to another, but, all the measured responses show comparable accuracy to the examples presented in this paper. This remarkable precision makes spread spectrum sounding highly appropriate for characterizing ultrawideband radio channels in a variety of situations, as well as for control of channel compensation schemes such as time reversal.

V. Conclusion

In this paper, we investigated accuracy of spread spectrum channel sounding based on deconvolution in typical LOS and NLOS indoor environments, in the later case up to 15 m propagation distance. An optical fiber link is used to facilitate synchronization of Tx-Rx in NLOS scenarios. Wideband probing waveforms provide higher levels of total transmitted power compared to ultrashort pulses, which results in a higher dynamic range. The AWG not only provides sufficient bandwidth for channel characterization over a frequency band spanning 2–12 GHz, but also provides the flexibility to choose different spread spectrum waveforms for sounding. We studied the accuracy of calculated impulse responses by comparing channel measurements obtained for PN sequence and chirp waveform excitation. Different experiments including LOS spiral and NLOS omni-directional antennas show more than 99 percent agreement between the chirp and PN excitation results. In another route to test the accuracy, time reversal has been carried out experimentally. Correlation coefficients between experimental and theoretical time reversal traces are on the order of 0.98. Our experiments clearly show that spread spectrum channel sounding can provide high accuracy measurements of the channel impulse response over the full UWB band. Furthermore, by exploiting the high quality impulse response data obtained, we are able to demonstrate time reversal experiments over a bandwidth, which to the best of our knowledge, has not previously been reported.

Acknowledgment

The authors would like to thank Prof. A. F. Molisch for his insightful comments, and our lab manager Dr. D. E. Leaird for his helpful technical assistance on this work. Any opinion, findings, and conclusions or recommendations expressed in this publication are those of the authors and do not necessarily reflect the views of the sponsors.

References

[1] A. F. Molisch, "Ultrawideband propagation channel," in *Proc. IEEE*, Feb. 2009, vol. 97, no. 2, pp. 353–371 .

[2] L. Yang and G. B. Giannakis, "Ultra-wideband communications—An idea whose time has come," *IEEE Signal Process. Mag.*, vol. 21, pp. 26–54, Nov. 2004.

[3] R. C. Qiu, H. Liu, and X. Shen, "Ultra-wideband for multiple access communications," *IEEE Commun. Mag.*, vol. 43, pp. 80–87, Feb. 2005.

[4] J. Romme and B. Kull, "On the relation between bandwidth and robustness of indoor UWB communication," presented at the UWBST'03 Conf., Nov. 2003.

[5] I. I. Immoreev and D. V. Fedotov, "Ultra wideband radar systems: Advantages and disadvantages," in *Proc. IEEE Ultra Wideband Syst. Technol. Conf.*, Baltimore, MD, May 2002, pp. 201–205.

[6] A. F. Molisch, "Ultrawideband propagation channels and their impact on system design," presented at the IEEE Conf. Meas., Antennas, Channels, EMC (MAPE), 2007.

[7] J. Karedal, S. Wyne, P. Almers, F. Tufvesson, and A. F. Molisch, "A measurement-based statistical model for industrial ultra-wideband channels," *IEEE Trans. Wireless Commun.*, vol. 6, no. 8, pp. 3028–3037, Aug. 2007.

[8] D. Cassioli, A. Durantini, and W. Ciccognani, "The role of path loss on the selection of the operating bands of UWB systems," in *Proc. IEEE Int. Symp. Personal, Indoor Mobile Radio Commun.*, 2004, pp. 2787–2791.

[9] P. Pagani and P. Pajusco, "Experimental analysis of the ultra wideband propagation channel over the 3.1 GHz–10.6 GHz frequency band," presented at the PIMRC, Helsinki, 2006.

[10] J. Keignart and N. Daniele, "Subnanosecond UWB channel sounding in frequency and temporal domain," in *Proc. IEEE Conf. Ultra Wideband Syst. Technol.*, 2002, pp. 25–30.

[11] W. Q. Malik, "Spatial correlation in ultrawideband channels," *IEEE Trans. Wireless Commun.*, vol. 7, pp. 604–610, Jul. 2008.

[12] S. S. Ghassenizadeh *et al.*, "A statistical path loss model for in-home UWB channels," in *Proc. UWBST*, 2002, pp. 59–64.

[13] R. J. M. Cramer, R. A. Scholtz, and M. Z. Win, "Evaluation of an ultra-wide-band propagation channel," *IEEE Trans. Antennas Propag.*, vol. 50, no. 5, pp. 561–70, May 2002.

[14] T. C.-K. Liu, D. I. Kim, and R. G. Vaughan, "A high-resolution, multi-template deconvolution algorithm for time-domain UWB channel characterization," *Can. J. Electr. Comput. Eng.*, vol. 32, no. 4, pp. 207–213, 2007.

[15] N. Alsindi, D. Birru, and D. Wang, "Ultra-wideband channel measurement characterization for wireless magnetic resonance imaging applications," presented at the 41th Conf. Inform. Sci. Syst. (CISS'07), Baltimore, MD, Mar. 14–16, 2007, Johns Hopkins University.

[16] Z. Irahhauten1, J. Dacuna1, G. J. M. Janssen, and H. Nikookar, "UWB channel measurements and results for wireless personal area networks applications," in *Proc. Eur. Conf. Wireless Tech.*, Paris, France, Oct. 3–4, 2005.

[17] A. Muqaibel, A. Safaai-Jazi, A. Attiya, B. Woerner, and S. Riad, "Pathloss and time dispersion parameters for indoor UWB propagation," *IEEE Trans. Wireless Commun.*, vol. 5, no. 3, pp. 550–559, Mar. 2006.

[18] J. R. Klauder, A. C. Price, S. Darlington, and W. J. Albersheim, "The theory and design of chirp radars," *Bell Sys. Tech. J.*, vol. 39, no. 4, pp. 745–820, Jul. 1960.

[19] R. Zetik, J. Sachs, and R. S. Thomä, "UWB short-range radar sensing," *IEEE Instrum. Meas. Mag.*, vol. 10, no. 2, Apr. 2007.

[20] S. Zhou, G. B. Giannakis, and A. Swami, "Digital multi-carrier spread spectrum versus direct sequence spread spectrum for resistance to jamming and multipath," *IEEE Trans. Commun.*, vol. 50, no. 4, pp. 643–655, Apr. 2002.

[21] J. Schoukens and R. Pintelon, *Identification of Linear Systems—A Practical Guideline to Accurate Modeling*. Oxford, U.K.: Pergamon Press, 1991.

[22] A. Richter, "Estimation of Radio Channel Parameters: Models and Algorithms," Ph.D. dissertation, Technische Universitat Ilmenau, Ilmenau, Germany, 2005.

[23] D. V. Sarwate and M. B. Pursley, "Crosscorrelation properties of pseudorandom and related sequences," *Proc. IEEE*, vol. 68, no. 5, pp. 593–619, May 1980.

[24] A. Hein, *Processing of SAR Data: Fundamentals, Signal Processing, Interferometry*. Berlin, Germany: Springer-Verlag, 2004.

[25] G. Janssen and J. Vriens, "High resolution coherent radio channel measurements using direct sequence spread spectrum modulation," in *Proc. 6th Mediterranean IEEE Electro Techn. Conf.*, 1991, vol. 1, pp. 720–727.

[26] A. Durantini, W. Ciccognani, and D. Cassioli, "UWB propagation measurements by PN—Sequence channel sounding," in *Proc. IEEE Int. Conf. Commun.*, Paris, France, 2004, pp. 3414–3418.

[27] A. Durantini and D. Cassioli, "Measurements, modeling and simulations of the UWB propagation channel based on direct-sequence channel sounding," *Wireless Comm. Mob. Comp. J.*, no. 5, pp. 513–523, 2005.

[28] R. Zetik, R. Thoma, and J. Sachs, "Ultra-wideband real-time channel sounder design and application," presented at the COST273 TD(03) 201, Prague, Czech Republic, 2003.

[29] J. Sachs, M. Kmec, R. Herrmann, P. Peyerl, and P. Rauschenbach, "An ultra-wideband pseudo-noise radar family integrated in SiGe:C," presented at the Int. Radar Symp. IRS 2006, Krakow, Poland, May 24–26, 2006.

[30] [Online]. Available: http://www.channelsounder.de/

[31] M. Kowatsch and J. T. Lafferl, "A spread-spectrum concept combining chirp modulation and pseudonoise coding," *IEEE Trans. Commun.*, vol. COM-31, no. 10, pp. 1133–1142, Oct. 1983.

[32] M. Fink, "Time reversal of ultrasonic fields—I: Basic principles," *IEEE Trans. Ultrason., Ferroelect., Freq. Contr.*, vol. 39, no. 5, pp. 555–566, Sep. 1992.

[33] D. Abbasi-Moghadam and V. T. Vakili, "Characterization of indoor time reversal UWB communication systems: Spatial, temporal and frequency properties," *Int. J. Commun. Syst.*, vol. 24, no. 3, pp. 277–294, Mar. 2011.

[34] I. H. Naqvi *et al.*, "Experimental validation of time reversal ultrawideband communication system for high data rates," *IEEE Trans. Antennas Propag.*, vol. 4, no. 5, pp. 643–650, May 2010.

[35] N. Guo, J. Q. Zhang, P. Zhang, Z. Hu, Y. Song, and R. C. Qiu, "UWB real-time testbed with waveform-based precoding," presented at the IEEE MILCOM'08, 2008.
[36] G. Tesserault, N. Malhouroux, and P. Pajusco, "Determination of material characteristics for optimizing WLAN radio," in *Proc. IEEE Eur. Conf. Wireless Technol.*, 2007, pp. 225–228.
[37] G. L. Li and P. K. L. Yu, "Optical intensity modulators for digital and analog applications," *J. Lightw. Technol.*, vol. 21, no. 9, pp. 2010–2030, Sep. 2003.
[38] M. K. Tsatsanis and G. B. Giannakis, "Blind estimation of direct sequence spread spectrum signals in multipath," *IEEE Trans. Signal Process.*, vol. 45, no. 5, pp. 1241–1252, May 1997.
[39] J. D. McKinney, D. Peroulis, and A. M. Weiner, "Time-domain measurement of the frequency-dependent delay of broadband antennas," *IEEE Trans. Antennas Propag.*, vol. 56, no. 1, pp. 39–47, Jan. 2008.
[40] J. D. McKinney, D. Peroulis, and A. M. Weiner, "Dispersion limitations of ultra-wideband wireless links and their compensation via photonically-enabled arbitrary waveform generation," *IEEE Trans. Microw. Theory Techn.*, vol. 56, no. 3, pp. 710–718, Mar. 2008.

Amir Dezfooliyan received the B.Sc. degree in electrical engineering from Sharif University of Technology, Tehran, Iran, in 2009. He is currently working toward the Ph.D. degree in electrical engineering at Purdue University, West Lafayette, IN.

Since 2009, he has been a Graduate Research Assistant with the Ultrafast Optics and Optical Fiber Communications Laboratory at Purdue University. His current research interests are wireless propagation, UWB communications, ultrafast optics, and optical pulse shaping.

Andrew M. Weiner (F'95) received the D.Sc. degree in electrical engineering from the Massachusetts Institute of Technology, Cambridge, in 1984.

Upon graduation, he joined Bellcore, first as a Member of Technical Staff and later as Manager of Ultrafast Optics and Optical Signal Processing Research. He moved to Purdue University, West Lafayette, IN, in 1992, and is currently the Scifres Family Distinguished Professor of Electrical and Computer Engineering. His research interests include ultrafast optics signal processing, and applications to high-speed optical communications and ultrawideband wireless. He is author of a textbook entitled *Ultrafast Optics* (Wiley, 2009), has published six book chapters and more than 250 journal articles, and is holder of over 10 U.S. patents.

Dr. Weiner is a Fellow of the Optical Society of America and is a Member of the U.S. National Academy of Engineering. He has won numerous awards for his research, including the Hertz Foundation Doctoral Thesis Prize (1984), the Adolph Lomb Medal of the Optical Society of America (1990), the Curtis McGraw Research Award of the American Society of Engineering Education (1997), the International Commission on Optics Prize (1997), the Alexander von Humboldt Foundation Research Award for Senior U.S. Scientists (2000), and the IEEE Photonics Society Quantum Electronics Award (2011). He is joint recipient, with J. P. Heritage, of the IEEE LEOS William Streifer Scientific Achievement Award (1999) and the OSA R.W. Wood Prize (2008), and has been recognized by Purdue University with the inaugural Research Excellence Award from the Schools of Engineering (2003) and with the Provost's Outstanding Graduate Student Mentor Award (2008). In 2009, he was named a U.S. Department of Defense National Security Science and Engineering Faculty Fellow. He has served as Cochair of the Conference on Lasers and Electro-optics and the International Conference on Ultrafast Phenomena, as Secretary/Treasurer of the IEEE Lasers and Electro-optics Society (LEOS), as a Vice-President of the International Commission on Optics (ICO), and as Chair of the National Academy of Engineering U.S. Frontiers of Engineering Meeting.